Pressure dependence of intermediate-range order and elastic properties of glassy Baltic amber

Sergey N. Tkachev,[1] Charlie M. Zoller,[2] Curtis Kenney-Benson,[3] Muhtar Ahart,[2] Russell J. Hemley,[2,4,5] Vladimir N. Novikov,[6] and Seiji Kojima[7,*]

[1]*Center for Advanced Radiation Sources, University of Chicago, Chicago, Illinois 60637, USA*
[2]*Department of Physics, University of Illinois Chicago, Chicago, Illinois 60607, USA*
[3]*HPCAT, X-ray Science Division, Argonne National Laboratory, Argonne, Illinois 60439, USA*
[4]*Department of Chemistry, University of Illinois Chicago, Chicago, Illinois 60607, USA*
[5]*Department of Earth and Environmental Sciences, University of Illinois Chicago, Chicago, Illinois 60607, USA*
[6]*Institute of Automation and Electrometry, Russian Academy of Sciences, Novosibirsk 630090, Russia*
[7]*Department of Materials Science, University of Tsukuba, Tsukuba, Ibaraki 305-8573, Japan*

(Received 21 January 2024; accepted 24 June 2024; published 2 August 2024)

Amber is a unique example of a fragile glass that has been extensively aged below its glass transition temperature, thus reaching a state that is not accessible under normal experimental conditions. We studied the medium-range order of Baltic amber by x-ray diffraction (XRD) at high pressures. The pressure dependences of the low-angle XRD intensity between 0 and 5 $Å^{-1}$ were measured from 0 to 7.3 GPa by the energy-dispersive XRD. The first diffraction peak at 1.1 $Å^{-1}$ and ambient pressure has a doublet structure consisting of the first sharp diffraction peak (FSDP) at 1.05 $Å^{-1}$ and the second feature at 1.40 $Å^{-1}$. The peak position and the width of the FSDP increase as the pressure increases, while the intensity of the FSDP decreases. Below $P_0 = 2.4$ GPa, the rapid increase of the FSDP peak position was observed, while above P_0, the gradual increase was observed. Below P_0, voids and holes in a relatively low-density state are suppressed, whereas above P_0, the suppression becomes mild. Such a change suggests the crossover from the low- to high-density state at P_0. There is a close correlation between the pressure dependence of XRD and previously reported sound velocity results. The correlation between the mean-square fluctuation of the shear modulus on the nanometer scale and fragility in amber and other glass formers is also discussed.

DOI: 10.1103/PhysRevE.110.024501

I. INTRODUCTION

Many liquids can be supercooled and undergo a liquid-glass transition at a glass transition temperature T_g. Upon cooling a liquid, the main structural relaxation time τ_α or viscosity η rapidly increases toward T_g and reaches at $\tau_\alpha = 100$ s or $\eta = 10^{13}$ poise at T_g. The concept of fragility was introduced based on the temperature dependence of the main structural relaxation time (or viscosity) [1]. That of typical strong glass obeys the Arrhenius law, while that of typical fragile liquid obeys the Vogel-Fulcher-Tammann law [2]. As a more quantitative measure of different levels of fragility, the fragility index m is defined by

$$m = \left[\frac{d\log_{10}\tau_\alpha}{d\left(\frac{T_g}{T}\right)}\right]_{T=T_g}. \tag{1}$$

The range of m is from 17 for very strong glasses to >100 for very fragile ones [3].

Crystal structures have a translational symmetry due to the long-range structural order, whereas glasses have no long-range structural order, but may exhibit medium-range order (MRO) on the scale of several nanometers [4–6]. Covalent network glasses can exhibit structural order over both short- and medium-length scales, the latter reaching 20 Å or so. MRO is characterized by the first sharp diffraction peak (FSDP) in the static structure factor $S(Q)$, where Q is the wave vector in neutron and x-ray diffraction (XRD) measurements [7]. It is proposed that the FSDP of network glasses and liquids is a prepeak in the concentration-concentration structure factor due to the chemical ordering of interstitial voids around cation-centered clusters in the structure [5]. A real-space ordering with MRO in a reciprocal space is given by

$$L_m = \frac{2\pi}{Q_1}, \tag{2}$$

and the static structure correlation length is defined by

$$L_c = \frac{2\pi}{\Delta Q}, \tag{3}$$

where Q_1 and ΔQ are the peak position and the peak width of the FSDP, respectively [7–11]. The temperature and pressure dependences of the FSDP intensity and its peak position were discussed according to various models. The temperature and pressure dependences of the FSDP in silica glass were quantitatively interpreted by the void-based model [12]. The FSDP of alkali borate glasses was attributed to the periodicity of boundaries of nanovoids homogeneously distributed in the

*Contact author: kojima@ims.tsukuba.ac.jp

network [13]. In chalcogenide glasses, it was reported that the FSDP corresponds to void-species nanostructure [14]. The doublet of FSDP of hydrogen-bonded water was assigned to the position of the first peak in the low-density (LD) and high-density (HD) forms of amorphous ice [15]. The FSDP and MRO of covalently bonded glasses have been extensively studied, while the study of those of organic glasses is still not enough. The temperature dependence of the width of the FSDP was analyzed in many kinds of glasses [16]. It was found that the width of the FSDP correlates with fragility, and it is significant in high-fragility liquids. Therefore, the study of the pressure dependence of the FSDP in fragile organic glass is important.

Glasses are nonequilibrium states whose microscopic properties vary depending on their thermal history. Amber is formed via a fossilization process by cross-linking of the original organic resin via free radical polymerization [17]. Amber is a very complex organic polymer/copolymer material formed from plant resins that have aged for many million years at temperatures well below T_g [18,19], thus reaching a thermodynamically stable state that is not accessible under normal experimental conditions [20]. Anderson *et al.* [18] reported a classification of fossil resins, and Baltic amber belongs to the Class I category. The bulk of Baltic amber consists of a polymer of labdatrienoid compounds including communic acid and communal with its hydroxyl groups partially succinylated. Amber also contains a few percent of many other compounds such as terpinol, succinate, and hemisuccinate esters [21]. The density of Baltic amber is 1.0–1.1 g/cm^3, and its refractive index is 1.54. The melting temperature is 250–300 °C, and the glass transition temperature is 182 °C [20]. It is a typical fragile glass with a fragility index of 90 [22]. The MRO of structural disorder in Baltic amber glass has not yet been studied.

In this paper, energy-dispersive XRD was studied in Baltic amber glass with high fragility using a Paris-Edinburgh press at Sector 16-BM-B (HPCAT) of the Advanced Photon Source (APS), Argonne National Laboratory. The pressure dependence of the diffraction spectra was measured up to 7.2 GPa. The structure correlation length L_c and medium-range length L_m were determined from the x-ray peak width and peak position of the FSDP, respectively. The correlation between the pressure dependences of the MRO and sound velocity determined by Brillouin scattering [23,24] is discussed.

II. EXPERIMENTAL METHODS

Baltic amber is a fossil pine resin of the Eocene Period and is about 40 million years old. Baltic amber imported from Lithuania was purchased from Planey Co., Ltd., Japan, and used without any thermal treatment. An experimental setup for high-pressure liquid structure studies with synchrotron XRD using the Paris-Edinburgh press has been installed at station 16-BM-B (HPCAT) of the APS, Argonne National Laboratory. By collecting energy-dispersive data with a synchrotron white beam at various 2θ angles, the present device allows us to obtain the structure factor $S(Q)$ over a wide range of $Q(=4\pi\sin\theta/\lambda)$ owing to the excellent angular accessibility of up to 9 ° in 2θ and that of high-energy photons well beyond 100 keV. We have successfully collected XRD data on Baltic amber with the scattering wave vector Q up to ∼5.0 Å^{-1} and pressure up to 7.3 GPa at room temperature [25,26]. The pressure dependences of longitudinal and transverse sound velocities have also been measured by the pulse-echo method [27]; however, these results will be published separately.

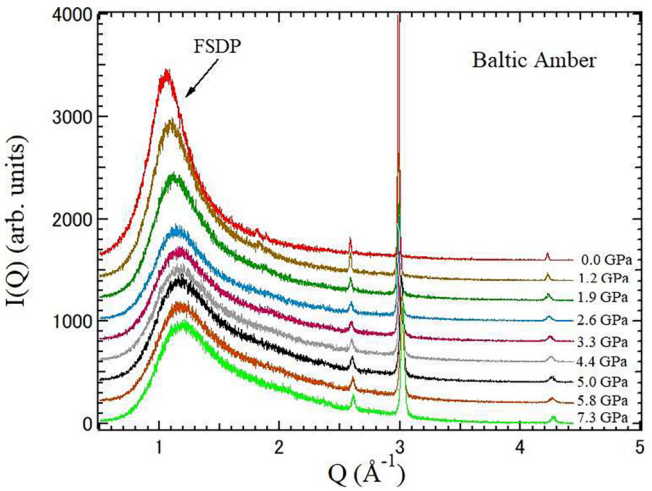

FIG. 1. Pressure dependence of diffraction intensity $I(Q)$. The sharp peaks at $Q = 2.6$, 3.0, and 4.3 Å^{-1} are the diffraction peaks from the pressure cell.

III. RESULT AND DISCUSSIONS

A. High-pressure XRD

Representative diffraction profiles $I(Q)$ as a function of the scattering wave vector Q are shown in Fig. 1. The broad first diffraction peak was observed at ∼1.1 Å^{-1}, and its intensity decreases as the pressure increases. The pressure dependence of the diffraction peak in a homogeneous glass is given by

$$\left(\frac{\partial I}{\partial P}\right)_T = \frac{\rho}{B}\left(\frac{\partial I}{\partial \rho}\right)_T, \tag{4}$$

where B and ρ are bulk modulus and density, respectively [12]. As the pressure increases, the void volume is concomitantly reduced, and hence, the density of glass is increased, and the peak intensity also decreases, leading to a negative sign for the term $(\partial I/\partial P)_T$. This behavior is like the temperature dependence of the diffraction peak intensity, which decreases as the temperature increases [28].

The first diffraction peak at ∼1.1 Å^{-1} has a doublet structure consisting of a sharp peak at 1.05–1.16 Å^{-1} and a weak shoulder at 1.23–1.56 Å^{-1}. The doublet peak reflects a heterogeneous structure such as the coexistence of LD and HD amorphous states caused by polyamorphism [1]. In silica glass, the strong-fragile transition was reported as polyamorphic behavior [29]. Under pressure, both peak positions of Baltic amber shift to higher wave vectors, and their widths increase. To fit the asymmetric shape of the diffraction peak, we checked a few versions of the fitting function for the structure factor. The first one is the sum of two Gaussian functions with maxima ∼1 and 1.5 Å^{-1}; the second one is the sum of two Lorentz functions; the third is the sum of a Gaussian for the first peak and a Lorentzian for the second

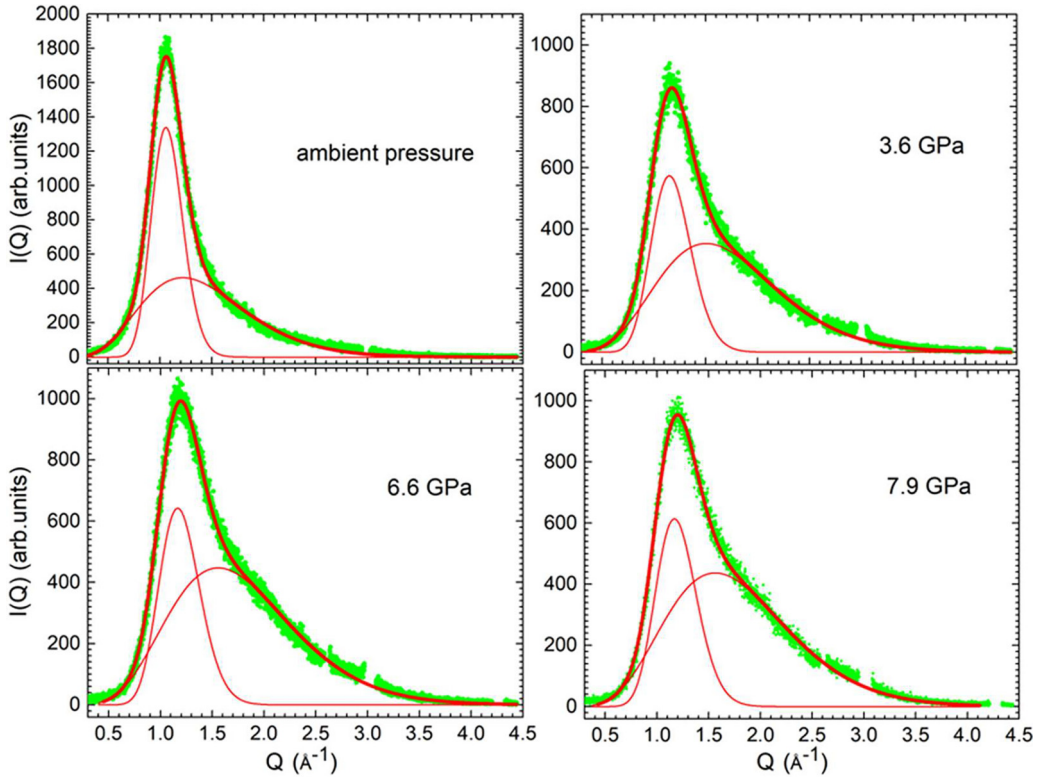

FIG. 2. Fits of $I(Q)$ by a sum of two Γ distributions. Representative fits at ambient pressure, 3.6, 6.6, and 7.9 GPa are shown. The individual contributions of the two peaks are shown by thin solid lines.

peak. These three fitting functions are qualitatively consistent with the shape of $I(Q)$, but all three clearly overestimate the existence of the second peak. They exhibit a pronounced shoulder not observed in the experimental data (see an example in Fig. S1 in the Supplemental Material [30]), although the shoulder is within the scatter of the experimental points. Moreover, the Lorentz function cannot describe the first peak at the base. A much better fit can be obtained if the two peaks themselves are asymmetrical in shape, namely, if they are right tailed. One of the common functions that is used in such cases is the two-parameter Γ distribution. It is a very flexible distribution that can provide diverse shape parameters, making it a perfect fit to different datasets. As an example, it describes well the size distribution of nanocrystalline domains [31].

To demonstrate the Γ distribution can be used in disordered materials, a few examples are listed below. (a) It describes the size distribution of the Voronoi cells associated with spatially randomly distributed particles (Poisson-Voronoi tessellation) [32]; (b) the Γ distribution is strongly associated with the grain size in a Poisson-Voronoi nucleation growth model [33], (c) granular materials and packing models [34], (d) the molecular weight distributions of polymers [35], and (e) volumes of the basins of attraction for mechanically stable particle packings [36]. We do not have a microscopic picture that justifies the application of the Γ distribution in the case of the diffraction peak in amber. Rather, it appeared to be the best choice among the common functions that we applied to fit the asymmetrical peak in our data.

The Γ distribution is described by the function:

$$I(Q) = B\left(\frac{Q}{Q_m}\right)^{\alpha}\exp\left(-\frac{\alpha Q}{Q_m}\right)$$

$$= \exp\left\{b+\alpha\left[\log_{10}\left(\frac{Q}{Q_m}\right)-\frac{Q}{Q_m}\right]\right\}. \qquad (5)$$

It corresponds to a slightly asymmetric peak with a maximum at $Q = Q_m$. The fit parameters b, α, Q_m, and the half width at half maximum (HWHM) of both peaks as well some other estimated parameters of the diffraction peaks at all pressures are given in Table S1 in the Supplemental Material [30]. The exponent α is in the range 50–35 for the first peak and 5.9–7.1 for the second for pressures from ambient to 7.9 GPa. The width at half maximum is determined by the difference between the two roots of the equation:

$$\Delta - \log_{10}(1+\Delta) = \frac{\log_{10}(2)}{\alpha}, \qquad (6)$$

where $\Delta = (Q - Q_m)/Q_m$. In our case, the HWHM can be approximated by the expression $\Delta Q \cong Q_m\,[2\log_{10}(2)/\alpha]^{1/2}$ which can be obtained from Eq. (5) by expanding $\log_{10}(1+\Delta)$ in powers of Δ up to Δ^2. This approximation has an accuracy of ∼0.1% for the first peak and ∼0.5% for the second peak. Representative fits at 10^{-4}, 3.6, 6.6, and 7.9 GPa are shown in Fig. 2, which also shows the individual contributions of the first and second peaks.

The resulting values of the peak positions, Q_1 and Q_2, are shown in Fig. 3(a) as a function of pressure. Both peak

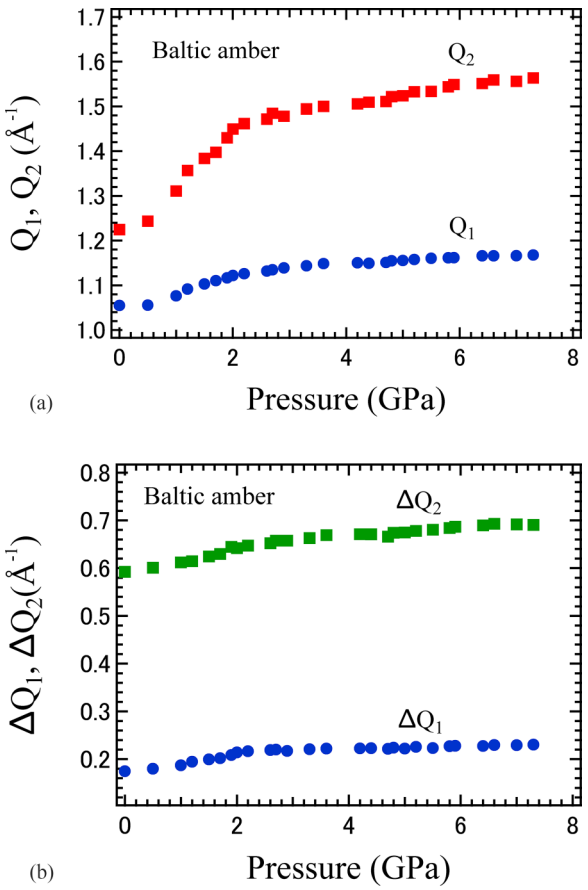

FIG. 3. Pressure dependences of (a) peak positions, Q_1, Q_2, and (b) half widths at the half maximum, ΔQ_1, ΔQ_2 of first sharp diffraction peak (FSDP) and second peak, respectively.

positions shift to higher Q from 1.05 to 1.16 Å^{-1} for FSDP and from 1.23 to 1.56 Å^{-1} for the second peak, with increasing pressure from ambient to 7.3 GPa. The pressure dependences of the HWHM for the two peaks are shown in Fig. 3(b). The width of FSDP, ΔQ_1, increases from 0.17 to 0.23 Å^{-1}, and the width of the second peak ΔQ_2 also increases from 0.59 to 0.69 Å^{-1} with increasing pressure.

The pressure dependence of FSDP peak position Q_1 of Baltic amber is compared with that of Kel F-800 polymer glass [37], as shown in Fig. 4. The value of Q_1 of Baltic amber is smaller than that of Kel F-800 polymer glass. Both Q_1's increase with pressure, while their rate of increase becomes small as the pressure increases. In the high-pressure region >3 GPa, dQ_1/dP (where P is the pressure) is nearly the same.

In a study of FSDP of poly(4-methyl-1-pentene) (P4MP1) under pressure, the intensity of the FSDP decreases with pressure, while that of the second peak increases. The ratio of the intensity of the FSDP to the second peak also decreases [38]. Abrupt changes were observed in the slope in this ratio at 0.7 kbar at 290 °C and in the position of the FSDP. The abrupt change was also studied by the specific-volume measurements, and it was attributed to the boundary between the LD and HD melts.

The pressure dependences of the peak intensities of the FSDP and the second peak and their ratio were also studied

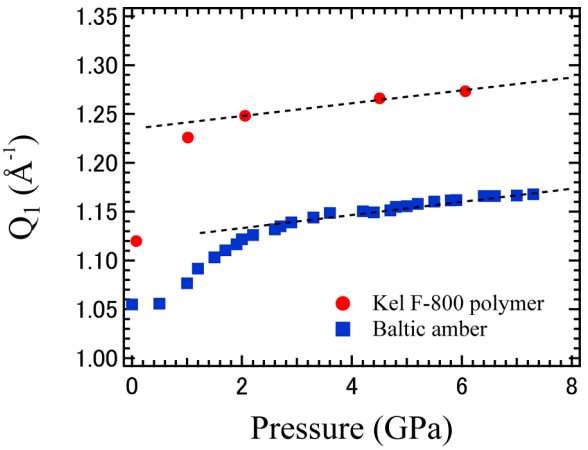

FIG. 4. The pressure dependences of Q_1 of Baltic amber and Kel F-800 polymer glass [37]. Dotted lines with the same dQ_1/dP are guides to the eyes.

in Baltic amber. As the pressure increases, the intensity of the FSDP decreases, while the intensity of the second peak increases. These results are like those of P4MP1. In glasses, the intensity of an nth diffraction peak $I(Q_n)$ is related to the local electron concentration of the nth structural unit, which has the periodicity related to a peak position Q_n. In the present result, the number density of the first structural units of FSDP decreases, while the number density of the second structural units of the second peak increases as the pressure increases. The pressure dependence of the ratio $I_R = I_2/I_1$ is shown in Fig. 5. The slope of the ratio I_R also shows a change at about $P_0 = 2.4$ GPa. This fact indicates that the crossover between the first structural units of FSDP and second structural units of the second peak occurs at ∼2.4 GPa. This crossover may be related to the transition from LD to HD states, which was observed in silica glass [39], amorphous GaSb [40], and amorphous ice [22]. In such transitions in tetrahedral network glass, a breaking of local tetrahedral symmetry occurs, whereas a different local symmetry breaking into a close-packed structure is necessary for the transition

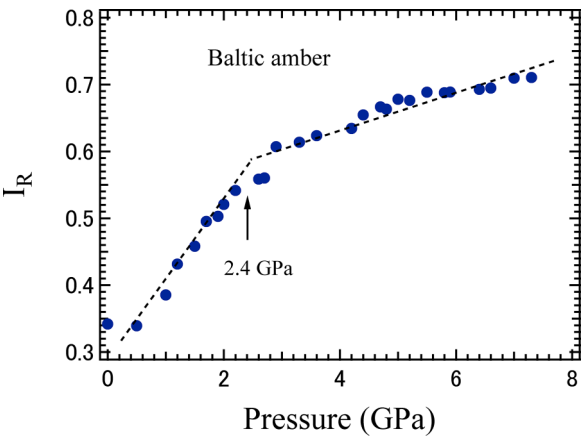

FIG. 5. The pressure dependence of the ratio $I_R = I_2/I_1$. The dotted linear line is a guide to the eyes. The change of slope of I_R occurs at ∼2.4 GPa.

of amber. The remarkable change in low pressures below P_0 suggests that voids and holes in a relatively LD state are being effectively suppressed. Above P_0 in a relatively HD state, the main change is the decrease in intermolecular distance. Similar pressure dependences were reported also in polyetherimide (PEI), polyethersulfone (PES), and polyvinyl chloride (PVC) [41]. The sound velocities and densities of these polymer glasses rapidly increased <2 GPa, followed by a slowly increase between 2 and 11 GPa.

The origin of the FSDP of polymers is related to the correlation between backbones. In P4MP1, the rapid decrease in the intensity of the FSDP with pressure indicates a disordering of backbone-backbone correlations. The shift of Q_1 to higher momentum transfers was attributed to a reduction of the void spaces between backbones. In contrast, polyethylene does not have any side chains to create a void structure, and it is significantly less compressible at low pressures [38]. The structure of amber is quite like that of polymers with phenyl ring side chains [42]. Therefore, the origins of rapid decreases of intensity and L_m in amber with side chains are attributed to the decrease in backbone-backbone correlations and the reduction of the void spaces between backbones, respectively.

B. Structural correlation length and MRO

Based on the FSDP, two length scales have been discussed. The scale of MRO, L_m, is the repetitive characteristic distance between structural units. Here, L_m is ∼4–6 times smaller than the value of the boson peak correlation length, which is defined by

$$L_b = \frac{V}{\nu_b}, \tag{7}$$

where V and ν_b are transverse sound velocity and boson peak frequency, respectively. Therefore, it corresponds to a much smaller size of the structural units related to a boson peak [43]. As the pressure increases, L_m decreases from 6.0 to 5.4 Å, as shown in Fig. 6(a). The pressure dependence of L_m of Baltic amber is compared with that of Kel F-800 polymer glass [44], as shown in Fig. 6(a). The value of L_m of Baltic amber is smaller than that of Kel F-800 polymer glass, and both lengths decrease as the pressure increases. At the same time, their pressure dependence becomes small as the pressure increases above $P_0 = 2.4$ GPa. The structure correlation length of a disordered structure, L_c, is known to be closely related to L_b [43]. The pressure dependence of L_c is shown in Fig. 6(b). It decreases with increasing pressure from 18.0 to 13.5 Å, by ∼20%, from ambient pressure to 7.3 GPa.

The ratio L_c/L_m indicates the relation between periodic structural units and the correlation length of the disorder. The ratio decreases with increasing pressure, from 3.02 to 2.53, as shown in Fig. 7. This fact indicates that L_c decreases faster than the distance between structural units. Therefore, the decrease of L_c is not just a trivial consequence of the decrease of the interdistance of backbone chains with increasing pressure. Applying pressure leads to a decrease in the number of atoms in the correlated nanoregion. Below about $P_0 = 2.4$ GPa, the ratio markedly decreases, which indicates the decrease of long-range disorder. Above ∼2.4 GPa, the change of ratio becomes small, and it indicates that the decrease rate of long-range disorder is like that of short-range disorder. For comparison, the intensity ratio I_1/I_2 is also plotted in Fig. 7. The pressure dependences of L_c/L_m and I_1/I_2 are similar. This

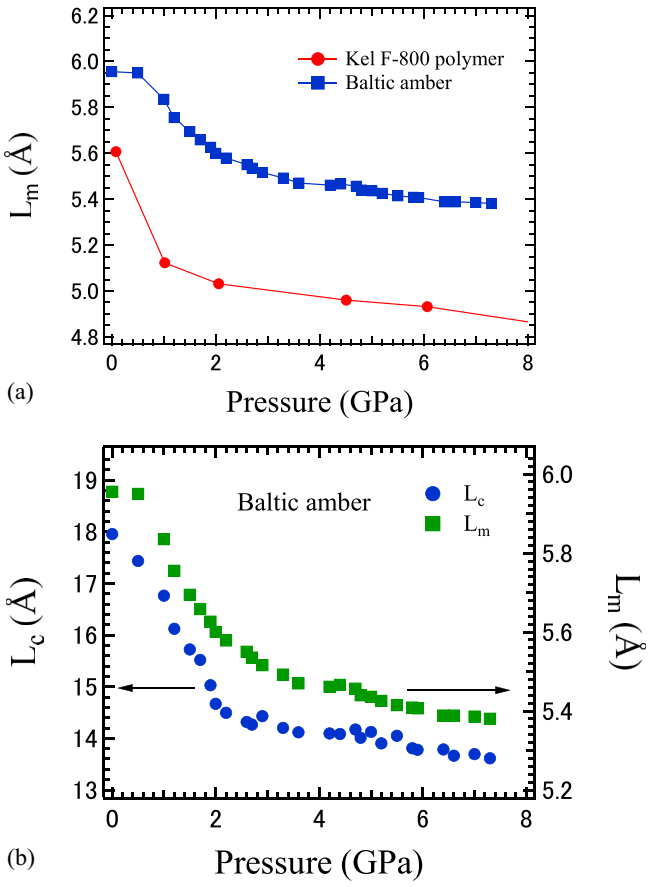

FIG. 6. (a) Comparison of the pressure dependence of L_m of Baltic amber with that of Kel F-800 polymer glass [44]. (b) The structure correlation length L_c is determined by the width of the first sharp diffraction peak (FSDP) and the scale of medium-range order (MRO) L_m by the position of the FSDP.

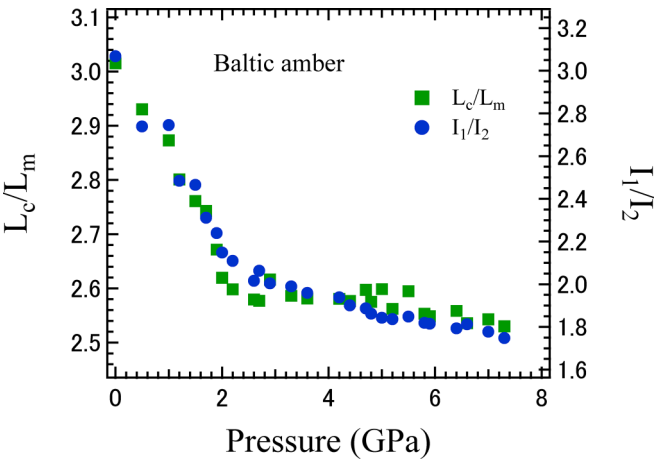

FIG. 7. The ratio of the structure correlation length and the scale of medium-range order (MRO) as a function of pressure. For the comparison, the intensity ratio I_1/I_2 is also plotted.

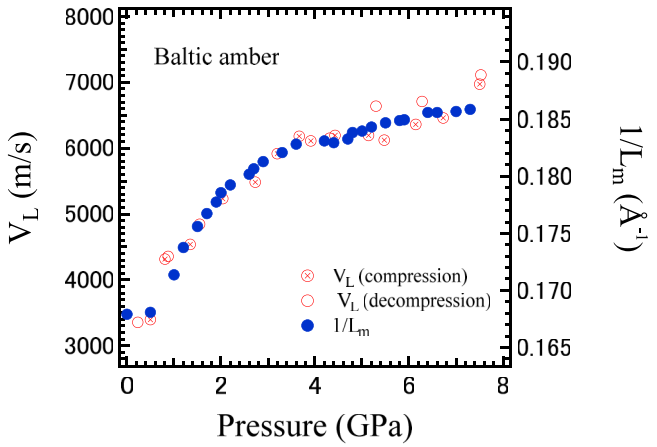

FIG. 8. Correlation of longitudinal velocity V_L and $1/L_m$ under pressure.

fact indicates that the main part of L_c may consist of the second structural units related to the second peak, while the main part of L_m may consist of the first structural unit related to the FSDP. For detailed analysis, further investigations are needed, such as studying broad spectra of $I(Q)$.

C. Correlation between FSDP, structure, and elastic properties

Structural disorder of glassy materials is closely related to their elastic properties. The strong correlation between the FSDP position and compressional sound velocity V_p or Poisson's ratio has been reported in SiO_2 glass [27]. This result implies that the change of V_p or Poisson's ratio is mainly influenced by intermediate-range ordering rather than short-range ordering in these structures.

The result of FSDP for Baltic amber is compared with the sound velocities determined by Brillouin scattering [23,24]. The value of V_L determined by Brillouin scattering in the gigahertz range is close to the high-frequency limit of velocity, and the dispersion of velocity by the structural relaxation is not included. The correlation in Fig. 8 suggests that V_L is nearly proportional to $1/L_m$. Here, V_L is equal to $(L/\rho)^{0.5}$, where L is the longitudinal modulus and ρ is the density. The dominant bonds in amber are van der Walls bonds, and the hydrogen bonds are partially included. The L decreases much faster than the density, and this correlation may hold accidentally. It is not a universal relation in glasses but a special correlation in amber.

In the present measurement at Argonne National Laboratory, not only XRD but also ultrasonic pulse-echo measurement in the megahertz range on longitudinal and transverse velocity were simultaneously measured. However, the ultrasonic measurement needs detailed analysis of the multiple reflections of ultrasonic echo waves inside a very small sample in the high-pressure cell. Such an analysis is not yet finished. We will discuss the physics of the correlation between all elastic moduli and diffraction data and the dispersion of velocity in the megahertz and gigahertz range in another paper.

In Refs. [43,45], the mean-square fluctuation of the shear modulus on the nanometer scale in various glass $\langle(\Delta G/G)^2\rangle$ was estimated using the heterogeneous elasticity theory and the Ioffe-Regel criterion for the transverse vibrations in glasses. A correlation between $\langle(\Delta G/G)^2\rangle$ and fragility of glass formers was found on the nanometer scale, which corresponds to the characteristic of the boson peak vibrations. Higher fragility corresponds to lower $\langle(\Delta G/G)^2\rangle$, i.e., to more homogeneous nanostructure. In this theory, to estimate $\langle(\Delta G/G)^2\rangle$, one needs to know the longitudinal and transverse sound velocities v_l and v_t, the structure correlation radius L_c, and the boson peak frequency ω_b. It was shown that

$$\langle(\Delta G/G)^2\rangle = \frac{L_b^3}{32\pi^4 L_c^3 f}, \tag{8}$$

where $L_b = 2\pi v_t/\omega_b$, in which L_b is the wavelength of the transverse acoustical vibration with the frequency of the boson peak, and f is a dimensionless function of the ratios L_b/L_c and v_t/v_l. The exact expression of this function is derived in Refs. [45,46]. The data on $v_t = 1.6$ km/s and $v_l = 2.71$ km/s for Baltic amber are known from Ref. [24], and for L_c in this paper, we get 18 ± 1 Å from the width of the FSDP at the ambient pressure. We note that this value of L_c is in reasonable agreement with the correlation length of the shear modulus fluctuations $\xi = 21 \pm 1$ Å found in pristine Spanish amber using the heterogeneous elasticity theory [48] fit of the boson peak. To find the dynamical length L_b, one needs to know the boson peak frequency in amber. We take $\omega_b = 1.5$ meV, as in Spanish amber [47]. In this case, $L_b = 27.7$ Å. The ratio $L_b/2L_c = 0.77$ is in good agreement with the general correlation of $L_b/2L_c$ with fragility for various glasses, as shown in Fig. 1 of Ref. [45]. With these parameters, L_b, L_c, v_t, and v_l, the function f in Eq. (8), according to its definition in Ref. [45], is equal to 0.0115, and $\langle(\Delta G/G)^2\rangle = 0.10$. This value corresponds well to the correlation between $\langle(\Delta G/G)^2\rangle$ on the nanometer scale and fragility in glasses of

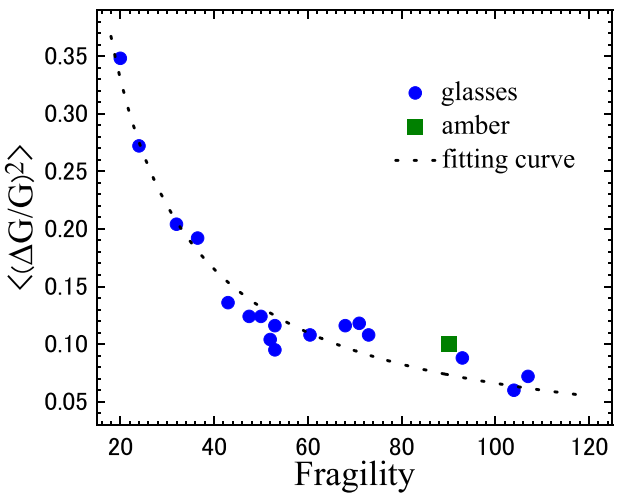

FIG. 9. The correlation between the mean-square fluctuation of the shear modulus on the nanometer scale and fragility in glass formers of different chemical positions and types of bonding, including glasses with covalent and hydrogen bonding, and molecular and metallic glasses [45] (blue circles). The data for amber of this paper are shown by a green square. The dotted line is inverse linear dependence $\sim m^{-1}$. The best-fit value gives the exponent -1.004 ± 0.054.

different chemical composition and type of bonding, found in Refs. [39,40]. Figure 9, which includes data from Ref. [45], includes the point that corresponds to amber (green square). The fragility of amber is about $m = 90$ [48].

IV. CONCLUSIONS

Pressure dependences of the low-angle XRD between 0 and 5 $Å^{-1}$ were measured on Baltic amber up to 7.3 GPa. The peak positions and the widths of the FSDP and the second peak increase as the pressure increases. The intensity of the FSDP decreases while that of the second peak increases. Below 2.4 GPa, the rapid increase of the FSDP peak position was observed, while above $P_0 = 2.4$ GPa, the more gradual increase was found. The remarkable change at P_0 suggests that voids and holes in a relatively LD state are being suppressed below P_0. This fact suggests the crossover from LD to HD states occurs at P_0. The pressure dependences of the MRO and the structure correlation length were determined from the peak position and the width of the FSDP, respectively. The correlation between pressure dependences of the MRO and the longitudinal sound velocity reported in Ref. [23] is found. This is also the evidence of correlations between the mean-square fluctuation of the shear modulus on the nanometer scale and fragility of amber and other glass-forming materials.

ACKNOWLEDGMENTS

This work was supported by the U.S. National Science Foundation under Grants No. DMR-DMR-2119308 and No. DMR-2118020, by the U.S. Department of Energy-National Nuclear Security Administration (DOE-NNSA) cooperative Agreement No. DE-NA-0003975 (Chicago/DOE Alliance Center, CDAC), and by Extreme EnErgy Density (EXEED), an Army HBCU/MI Center of Excellence at the University of Illinois Chicago, under Grant No. W911NF2110275 from the Army Research Office. X-ray experiments were performed at HPCAT (Sector 16), Advanced Photon Source (APS), Argonne National Laboratory (ANL). HPCAT operations are supported by DOE-NNSA's Office of Experimental Sciences. The APS is a DOE Office of Science User Facility operated for the DOE Office of Science by ANL under Contract No. DE-AC02-06CH11357. The work of VNN is supported by State Assignment No. 124041700106-2.

[1] C. A. Angell, J. Phys. Chem. Solids **49**, 863 (1988).
[2] D. H. Vogel, Phys. Z. **22**, 645 (1921).
[3] R. Boehmer, K. L. Ngai, C. A. Angell, and D. J. Plazek, J. Chem. Phys. **99**, 4201 (1993).
[4] G. Lucovsky and F. L. Galeener, J. Non-Cryst. Solids **35**, 1209 (1980).
[5] S. R. Elliot, Nature (London) **354**, 445 (1992).
[6] G. N. Greaves, A. L. Greer, R. S. Lakes, and T. Rouxel, Nat. Mat. **10**, 823 (2011).
[7] J. Als-Nielsen and D. McMorrow, *Elements of Modern X-Ray Physics* (John Wiley & Sons, New York, 2011).
[8] P. S. Salmon, Proc. R. Soc. Lond. A **445**, 351 (1994).
[9] P. H. Gaskell and D. J. Wallis, Phys. Rev. Lett. **76**, 66 (1996).
[10] P. S. Salmon, R. A. Martin, P. E. Mason, and G. J. Cuello, Nature (London) **435**, 75 (2005).
[11] J. M. Zaug, A. K. Soper, and S. M. Clark, Nat. Mater. **7**, 890 (2008).
[12] S. R. Elliot, J. Non-Crys. Solids **182**, 40 (1995).
[13] C. Crupi, G. Carini, M. Gonzalez, and G. D'Angelo, Phys. Rev. B **92**, 134206 (2015).
[14] T. S. Kavetskyy, O. I. Shpotyuk, and V. T. Boyko, J. Phys. Chem. Solids **68**, 712 (2007).
[15] D. R. Barker, M. Wilson, P. A. Madden, N. N. Medvedev, and A. Geiger, Phys. Rev. E **62**, 1427 (2000).
[16] D. N. Voylov, P. J. Griffin, B. Mercado, J. K. Keum, M. Nakanishi, V. N. Novikov, and A. P. Sokolov, Phys. Rev. E **94**, 060603(R) (2016).
[17] H. Kimura, Y. Tsukada, H. Mita, Y. Yamamoto, R. Chujo, and T. Yukawa, Bull. Chem. Soc. Jpn. **79**, 451 (2006).
[18] K. B. Anderson, R. E. Winans, and R. E. Botto, Org. Geochem. **18**, 829 (1992).
[19] G. O. Poinar, Geol. Today **14**, 154 (1998).
[20] J. Zhao, E. Ragazzi, and G. B. McKenna, Polymer **54**, 7041 (2013).
[21] J. S. Mills, R. White, and L. J. Gough, Chem. Geol. **47**, 15 (1984).
[22] O. Mishima, J. Chem. Phys. **100**, 5910 (1994).
[23] K. H. Oh, Y. H. Ko, S. Kojima, and J.-H. Ko, J. Kor. Phys. Soc. **77**, 773 (2020).
[24] S. N. Tkachev, M. Ahart, V. N. Novikov, and S. Kojima, Jpn. J. Appl. Phys. **60**, SDDA04 (2021).
[25] S. Klotz, G. Hamel, and J. Frelat, High Press. Res. **24**, 219 (2004).
[26] A. Yamada, Y. Wang, T. Inoue, W. Yang, C. Park, T. Yu, and G. Shen, Rev. Sci. Instrum. **82**, 015103 (2011).
[27] Y. Kono, C. Park, T. Sakamaki, C. Kenny-Benson, G. Shen, and Y. Wang, Rev. Sci. Instrum. **83**, 033905 (2012).
[28] H. Iyetomi, P. Vashishta, and R. K. Kalia, Phys. Rev. B **43**, 1726 (1991).
[29] I. Saika-Voivod, P. H. Poole, and F. Sciortino, Nature (London) **412**, 514 (2001).
[30] See Supplemental Material at http://link.aps.org/supplemental/10.1103/PhysRevE.110.024501 for additional data, including the figure (Fig. S1) with comparison of the fit with various fitting functions and the table with the fitting parameters and estimated parameters of the diffraction peaks at various pressures (Table S1).
[31] *Diffraction Analysis of the Microstructure of Materials*, edited by E. J. Mittemeijer and P. Scardi (Springer-Verlag, Berlin, 2004), Chaps. 3 and 5.
[32] J.-S. Ferenc and Z. Néda, Phys. A: Stat. Mech. Appl. **385**, 518 (2007).
[33] E. Pineda, V. Garrido, and D. Crespo, Phys. Rev. E **75**, 040107(R) (2007).
[34] T. Aste and T. Di Matteo, Phys. Rev. E **77**, 021309 (2008).
[35] N. H. Williamson, M. Nydén, and M. Röding, J. Magn. Reson. **267**, 54 (2016).
[36] S. S. Ashwin, J. Blawzdziewicz, C. S. O'Hern, and M. D. Shattuck, Phys. Rev. E **85**, 061307 (2012).

[37] E. Stavrou, M. Ahart, M. F. Mahmood, and A. F. Goncharov, Sci. Rep. **3**, 1290 (2013).
[38] A. Chiba, N. Funamori, K. Nakayama, Y. Ohishi, S. M. Bennington, S. Rastogi, A. Shukla, K. Tsuji, and M. Takenaka, Phys. Rev. E **85**, 021807 (2012).
[39] Y. Kono, K. Ohara, N. M. Kondo, H. Yamada, S. Hiroi, F. Noritake, K. Nitta, O. Sekizawa, Y. Higo, Y. Tange *et al.*, Nat. Commun. **13**, 2292 (2022).
[40] V. A. Sidorov, V. V. Brazhkin, L. G Khvostantsev, A. G. Lyapin, A. V. Sapelkin, and O. B. Tsiok, Phys. Rev. Left. **73**, 3262 (1994).
[41] K. H. Oh, Y.-H. Ko, and K.-J. Kim, Physica B **576**, 411722 (2020).
[42] J. Zhao and G. B. McKenna, Polymer **55**, 2246 (2014).
[43] A. P. Sokolov, A. Kisliuk, M. Soltwisch, and D. Quitmann, Phys. Rev. Lett. **69**, 1540 (1992).
[44] A. S. Benjamin, M. Ahart, S. A. Gramsch, L. L. Stevens, E. B. Orler, D. M. Dattelbaum, and R. J. Hemley, J. Chem. Phys. **137**, 014514 (2012).
[45] V. N. Novikov, Phys. Rev. E **106**, 024611 (2022).
[46] S. Kojima, V. N. Novikov, M. Kofu, and O. Yamamuro, Phys. Status Solidi B **257**, 2000073 (2020).
[47] E. A. A. Pogna, A. I. Chumakov, C. Ferrante, M. A. Ramos, and T. Scopigno, J. Phys. Chem. Lett. **10**, 427 (2019).
[48] J. Zhao, S. L. Simon, and G. B. McKenna, Nat. Commun. **4**, 1783 (2013).